Effect of Stress Type on the Oxide Layer Properties of Alloy 600MA and 690TT in Simulated Secondary Water

Byung Joon Bae[a,b], Jeoh Han[a], Jongsup Hong[b], Do Haeng Hur[a*]
[a]*Materials Safety Technology Development Division, Korea Atomic Energy Research Institute, 989-111 Daedeok-daero, Yuseong-gu, Daejeon, 34057, Republic of Korea*
[b]*Division of Mechanical Engineering, Yonsei University, 50 Yonsei-ro Seodaemungu, Seoul, 03722, Republic of Korea*
*Corresponding author: dhhur@kaeri.re.kr

1. Introduction

Seamless tubing made of Alloy 600 and Alloy 690 has been used for steam generator (SG) tubes in reducing and nearly impurity-free secondary water conditions [1]. And they are protective material from corrosion damages such as stress corrosion cracking, pitting, and intergranular attack. Many studies on secondary side degradation of SG tubes have been carried out to verify that corrosion of SG tubes is accelerated by impurities [2,3], surface condition [4] and stress [5].

Among these, stress leads to less resistance to corrosion behavior of Ni-based alloys. The notable results obtained from numerous studies on effect of stress on corrosion can be followed: the increasing crack growth rate with increasing applied stress [5]; selective oxidation of chromium [6].

It is noticeable that the corrosion damage by impurities occurs after most surfaces of SG tubes are covered with deposits and oxide layers under diverse stress conditions. However, most of investigations are not considered oxide layers covering the material before corrosion damage occurs. Therefore, it is necessary to evaluate the characteristics of oxide layer under stress condition.

The objective of this research is to understand the effect of stress type on the oxide layer formation of SG tube material in simulated secondary water. To achieve this goal, three different stress types of specimen were prepared and corrosion test is performed at 340 ℃ for 1000 h in simulated secondary water.

2. Experimental Methods

2.1. Preparation of Specimens

Every specimen was prepared from Alloy 600 and 690 plates. Alloy 600 were mill annealed (MA) at 950 ℃ for 2 h and air cooled to relieve stress. Alloy 690 were thermally treated (TT) at 715 ℃ for 10 h after mill annealing. The chemical compositions of specimens are shown in Table 1.

Test specimens were used in two different types (U-bend type and plate type). U-bend type specimens are for stressed condition and plate type specimens are for stress-free condition. Before bending, they were grounded by silicon carbide paper from #600 grits to #1000 grits to achieve in the same surface condition. These were ultrasonically cleaned in acetone. The U-bend type specimens were prepared according to the guideline provided by ASTM G30-97 as shown in Fig. 1.

Table. 1. Chemical compositions of test materials (wt. %).

	Ni	Cr	Fe	Mn	C	Si	Cu
Alloy 600MA	75.2	15.03	8.23	0.39	0.048	0.08	0.01
Alloy 690TT	Bal.	28.0	10.2	0.3	0.02	0.1	0.01

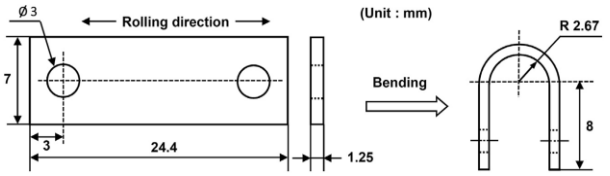

Fig. 1. Dimensions of a U-bend type specimen.

2.2. Corrosion Test

Corrosion test was operated in a secondary water recirculating loop system shown in Fig. 2. The test solution was deionized water. Its pH was adjusted by ethanolamine to 9.0 at 25 ℃. To eliminate the effects of oxygen, dissolved oxygen of solution in the feed tank and pH control tank was controlled to be less than 5 ppb using high purity nitrogen gas. Different two types of specimens were loaded on a specimen holder made of Alloy 600 material to avoid any galvanic corrosion between the specimens and holder. The test solution circulated at 200 cc/min and maintained at 340 ℃ under 150 bars for 1000 h.

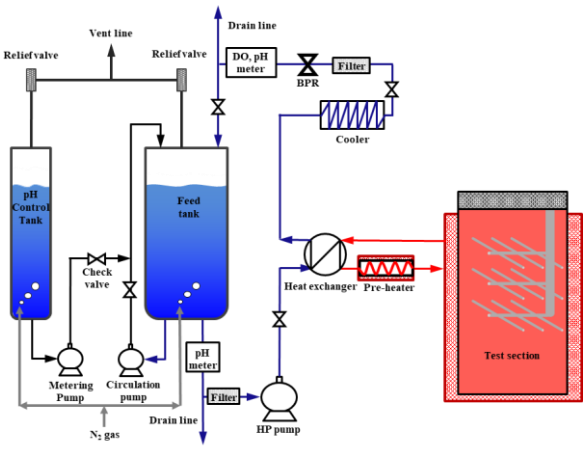

Fig. 2. Schematic diagram of the loop system for the corrosion test.

2.3. Oxide layer Analysis

After the test, the morphology of oxide layers and particles formed on the specimens was observed using scanning electron microscopy (SEM). The focus ion beam milling technique was used to produce samples for transmission electron microscopy (TEM). For the specimen under tensile stress condition, the TEM sample was produced at the apex of the U-bend specimen, at which the strain rate of the specimen was maximum. The distribution of chemical species was observed by using mapping and line analyses of energy dispersive X-ray spectroscopy (EDS) attached to the TEM.

3. Result and Discussion

Fig. 3 shows the SEM morphologies of the outer oxide films formed on Alloy 600MA and 690TT. The surface morphologies of outer oxide films were significantly changed between tensile stress condition and other stress conditions. The outer surface was covered with numerous polyhedral oxide particles mostly. However, as shown in Fig. 3 (a) and (d), oxide particles with a diameter of nealy 2 μm were observed more frequently on the specimen under the tensile stress condition on both Alloy 600MA and 690TT compared with other stress conditions. Comparing (b) and (e), the average diameter of oxide particles covering the surface of Alloy 600MA is approximately 0.5 μm, much bigger than that of Alloy 690TT.

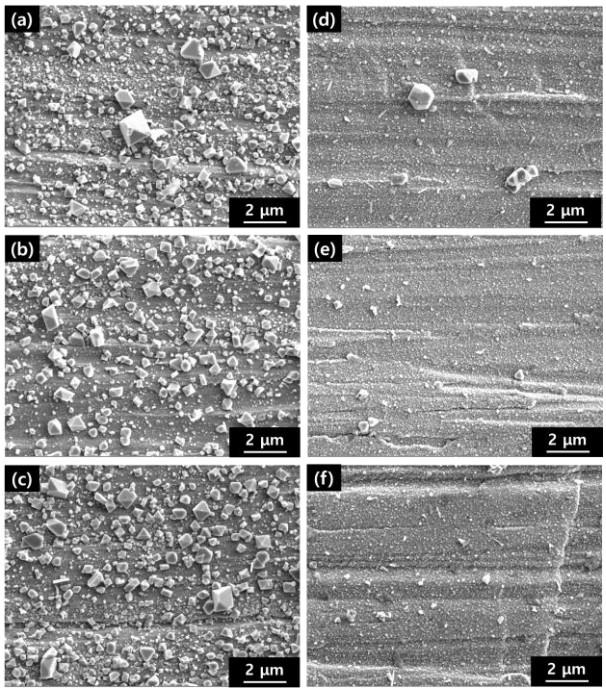

Fig. 3. SEM images of specimens after 1000 h corrosion test: Alloy 600 specimens under (a) tensile stress condition, (b) stress-free condition, (c) compressive stress condition, Alloy 690 specimens under (d) tensile tensile stress condition, (e) stress-free condition and (f) compressive stress condition.

Figs. 4 and 5 show the STEM-EDS mapping images of the surface oxide layer of Alloy 600MA and Alloy 690TT, respectively, under the different three stress conditions. In Fig. 4, Cr-rich oxide layer was observed in every condition. However, the inner oxide layer formed under tensile stress condition was thicker than that formed under other stress conditions on Alloy 600MA.

However, as shown in Fig. 5, Cr-rich inner oxide layer was observed but thickness of inner oxide layer was not dependent on the stress conditions.

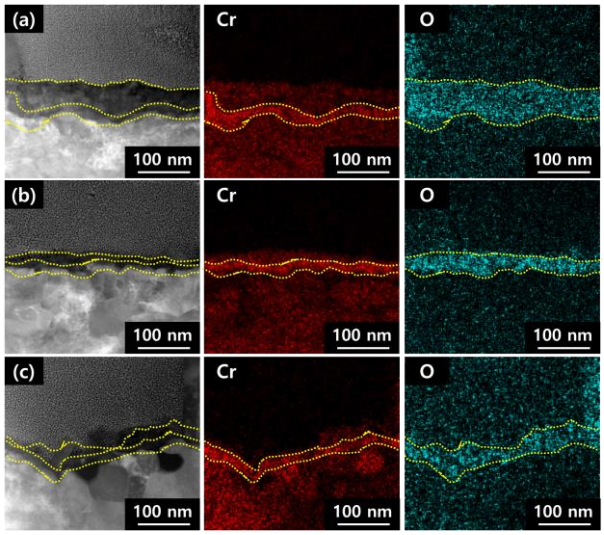

Fig. 4. STEM-EDS mapping image of Alloy 600MA specimens after 1000 h corrosion test: (a) tensile stress condition, (b) stress-free condition, (c) compressive stress condition.

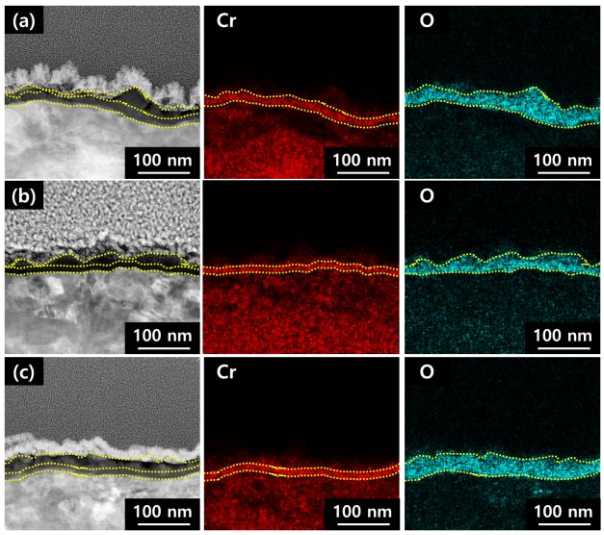

Fig. 5. STEM-EDS mapping image of Alloy 690TT specimens after 1000 h corrosion test: (a) tensile stress condition, (b) stress-free condition, (c) compressive stress condition.

Figs. 6 and 7 show STEM images and EDS line profiles across the surface oxide layers of Alloy 600MA and Alloy 690TT. The location and direction of the measurement were denoted with an arrow. As shown in Fig. 6, there was no dramatic difference about thickness

of Cr-rich layers and Cr-depleted layers depending on the stress type. However, the atomic percentage of chromium in Cr-rich oxide layer under tensile stress was approximately 60 at. % less than that under other conditions.

As shown in graph of Fig. 7, both thickness of Cr-rich layers and atomic percentage of chromium in Cr-rich oxide layer under every stress conditions show no difference between each other.

Chromium is well known as a resistant component to corrosion and directly related to corrosion damages [7,8]. Thus the lower chromium content of oxide layer under tensile stress condition could affect the corrosion of Ni-based alloy.

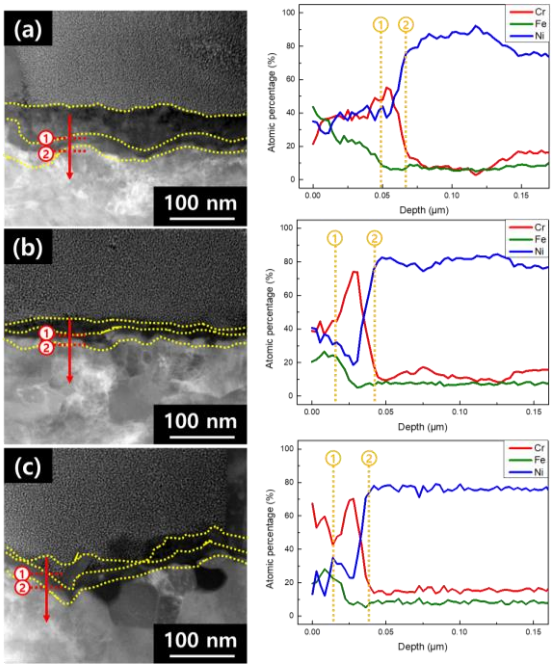

Fig. 6. STEM images and EDS line profiles on the outer oxide film of Alloy 600MA specimens after 1000 h corrosion test: (a) tensile stress condition, (b) stress-free condition, (c) compressive stress condition.

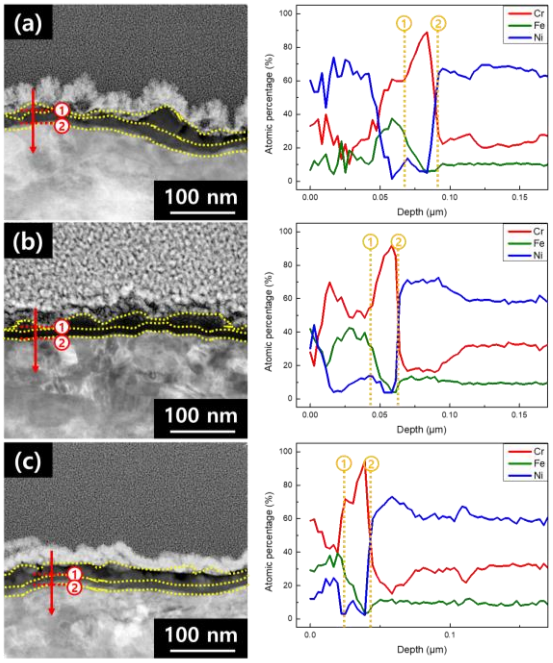

Fig. 7. STEM images and EDS line profiles on the outer oxide films of Alloy 690TT specimens after 1000 h corrosion test: (a) tensile stress condition, (b) stress-free condition, (c) compressive stress condition.

4. Conclusions

1) The oxide particles on the surface were polyhedral shape and nickel chromium ferrite in general. However oxide particles of diameter of nearly 2 μm in size were observed relatively more under the tensile stress condition of Alloy 600MA specimen, indicating that anodic dissolution was increased under the tensile stress condition.

2) On Alloy 600MA specimen, the inner oxide layer formed under tensile stress condition was thicker than that formed under stress-free condition. but inner oxide layer of Alloy 690TT under tensile stress condition, stress-free condition and compressive stress condition have no difference about thickness as Alloy 600MA. This indicates that oxygen penetration of Alloy 600MA was increased under the tensile stress condition.

3) The atomic percentage of chromium in Cr-rich oxide layer of Alloy 600MA under tensile stress was approximately 60 at. % less than that under other stress conditions. But that of Alloy 690TT have no difference with atomic percentage under different stress type conditions. As a result, the less atomic percentage of Cr-rich inner oxide layer under tensile stress conditions leads to less resistance to corrosion in simulated secondary water.

Acknowledgement

This work was supported by the National Research

Foundation (NRF) grant funded by the government of the Republic of Korea (NRF-2017M2A8A4015159).

REFERENCES

[1] EPRI, Pressurized Water Reactor Secondary Water Chemistry Guidelines -Revision 6, Electric Power Research Institute, Palo Alto, CA, USA, 2004, p. 1008224.
[2] B.T. Lu, J.L. Luo, Y.C. Lu, Passivity Degradation of Nuclear Steam Generator Tubing Alloy induced by Pb Contamination at High Temperature, Journal of Nuclear Materials, Vol.429, p305, 2012.
[3] D.H. Hur, M.S. Choi, D.H. Lee, M.H. Song, J.H. Han, Root Causes of Intergranular Attack in an Operating Nuclear Steam Generator Tube, Journal of Nuclear Material. Vol.375, p382, 2008.
[4] W.I. Choi, G.D. Song, S.H. Jeon, S.J. Kim, D.H. Hur, Magnetite-Accelerated Stress Corrosion Cracking of Alloy 600 in Water containing 100ppm Lead Oxide at 315 ℃, Journal of Nuclear Materials, Vol.522, p54, 2019.
[5] R.B. Rebak, Z. Szklarska-Smialowska, The Mechanism of Stress Corrosion Cracking of Alloy 600 in High Temperature Water, Corrosion Science, Vol.38, p971, 1996.
[6] G. Bertali, F.Scenini, M.G. Burke, The Effect of Residual Stress on the Preferential Intergranular Oxidation of Alloy 600, Corrosion Science, Vol.111, p. 494, 2016.
[7] T. Terachi, T. Yamada, T. Miyamoto, K. Arioka, K. Fukuya, Corrosion Behavior of Stainless Steels in Simulated PWR Primary Water-Effect of Chromium Content in Alloys and Dissolved Hydrogen-, Journal of Nuclear Science and Technology, Vol.45, p.975, 2008.
[8] F. Delabrouille, B. Viguier, L. Legras, E. Andrieu, Effect of the Chromium Content on the Corrosion of Nickel based Alloys in Primary Water of Pressurised Nuclear Reactors, Materials at High Temperatures, Vol.22, p287, 2005.